2011

DESIGN OF A LIQUID FUEL INJECTOR FOR ALTERNATIVE FUEL STUDIES IN AN ATMOSPHERIC MODEL GAS TURBINE COMBUSTOR

John Stevenson
Bucknell University

Follow this and additional works at: https://digitalcommons.bucknell.edu/honors_theses

Part of the Mechanical Engineering Commons

DESIGN OF A LIQUID FUEL INJECTOR FOR
ALTERNATIVE FUEL STUDIES IN AN ATMOSPHERIC MODEL
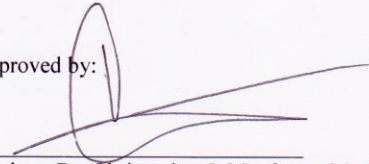**GAS TURBINE COMBUSTOR**

by

John Ernest Stevenson

Submitted to the Honors Council
For Honors in Mechanical Engineering

May 11, 2011

Approved by:

_____
Advisor: Dr. Christopher J. Mordaunt, Mechanical Engineering Dept.

Department Advisor: Dr. M. Laura Beninati, Mechanical Engineering Dept.

Department Chairperson: Dr. Charles Knisely, Mechanical Engineering Dept.

TABLE OF CONTENTS

LIST OF FIGURES

LIST OF TABLES

ABSTRACT

A new liquid-fuel injector was designed for use in the atmospheric-pressure, model gas turbine combustor in Bucknell University's Combustion Research Laboratory during alternative fuel testing. The current liquid-fuel injector requires a higher-than-desired pressure drop and volumetric flow rate to provide proper atomization of liquid fuels. An air-blast atomizer type of fuel injector was chosen and an experiment utilizing water as the working fluid was performed on a variable-geometry prototype. Visualization of the spray pattern was achieved through photography and the pressure drop was measured as a function of the required operating parameters. Experimental correlations were used to estimate droplet sizes over flow conditions similar to that which would be experienced in the actual combustor. The results of this experiment were used to select the desired geometric parameters for the proposed final injector design and a CAD model was generated. Eventually, the new injector will be fabricated and tested to provide final validation of the design prior to use in the combustion test apparatus.

Alphanumeric

AFR	air/fuel ratio
b, *c*, *d*, *e*, and *f*	coefficients used to balance the chemical equation
C_1, C_2	constants used in the O'Shaughnessy *et al.* correlation
C_xH_y	hydrocarbon fuel
CO	carbon monoxide
CO_2	carbon dioxide
d, d_F	jet diameter
$D^2(t)$	variation of droplet diameter as a function of time
D_0	initial droplet diameter
H	hydrogen
h	injector distance between fuel orifice and exit orifice of injector
K	evaporation constant
$\dot{m}$	mass flow rate of the liquid
MW_{air}	molecular weight of air
MW_{fuel}	molecular weight of fuel
N_2	nitrogen
O_2	oxygen
P	pressure
Q_A	volumetric flow rate of air
Q_L	volumetric flow rate of liquid
t	time
t_d	droplet lifetime
U_A	air velocity
U_R	velocity of the air relative to the liquid
V	voltage
x	number of carbon atoms in the fuel molecule
X_P	pressure demonstrated by voltage in pressure transducer
y	number of hydrogen atoms in the fuel molecule

Greek Letters

Δ	change in quantity
Φ	equivalence ratio
ρ, ρ_L	density of liquid
μ_L	dynamic viscosity of liquid
σ_L	surface tension of liquid

INTRODUCTION

The study of alternative fuels allows sources of future energy to be determined, and the ability to do such work in a controlled, safe environment is paramount to collecting and evaluating novel and accurate data. Liquid fuels, due to their increased energy density, present great potential for use as alternative fuels. The current injector used to test liquid fuels at Bucknell University's Combustion Research Laboratory (CRL) requires both a high pressure drop and a high volumetric flow rate to properly atomize liquid fuel. These requirements are hazardous and prohibit constructive combustion research. The objective of this work is to design a new liquid-fuel injector that will provide sufficient atomization of the fluid within reasonable pressure and volumetric flow limits such that it may safely be used in the CRL test apparatus. Additionally, the injector should be easy to disassemble and clean and is required to be easily manufacturable in Bucknell University's machine shop. Additionally, it is not an objective of the current study, but the ability to develop an injector that can be utilized in collaboration with the system at the Propulsion Engineering Research Center (PERC) at The Pennsylvania State University would be highly advantageous.

The following sections provide a brief background of the test apparatus at the CRL, some important relations in combustion and spray atomization, and a detailed description of the prototype injector testing and final injector design.

Combustion and Society

With increased concern over the environmental impact of fossil-fuel use and the role energy plays in national security, the importance of fuels which can be generated either from native resources, such as coal, or from biomass gasification of waste products has grown. Much of this interest is demonstrated with gaseous-fuel research, such as hydrogen, but there is also significant attention being paid to alternative liquid fuels. Many of these liquid-fuel studies investigate coal-derived or Fischer-Tropsch liquid fuels for use in various applications, particularly in the transportation and defense sectors [1,2].

Combustion Research at Bucknell University

The CRL has established the infrastructure to substantively test both gaseous and liquid alternative fuels [3]. The atmospheric combustor at Bucknell University (shown with a methane flame in Figure 1) is capable of burning these fuels with the capacity to record visual information of the flame's structure and pollutant emissions created during combustion. One of the CRL's research topics is the combustion of biogas in gas turbines for use in power generation with low-NO_x, lean-premixed combustors [4]. The CRL's combustion system was designed to be geometrically similar to the high-pressure, high-temperature apparatus operating at PERC to optimize collaboration between the two universities. However, although both the gaseous- and liquid-fuel

injectors used at the CRL and PERC are similar, the CRL's system operates at significantly lower mass flow rates due to the atmospheric operating conditions.

Figure 1. Methane flame in CRL atmospheric combustor.

The current issue with the CRL's system is its liquid-fuel injector: since the pressure and volumetric flow rate required to provide sufficient atomization of the fuel is so high, an excessive quantity of fuel is required for proper operation. To test liquid fuels at the CRL previously, a Delavan Model 46817-33HL injector was used [3]. This injector (Figure 2), however, has several features that make it undesirable for use in the CRL. First, the pressure in the injector required for a good spray pattern is significantly higher than the atmospheric pressure in the combustion chamber. Such a large pressure differential could cause a catastrophic failure of the system.

Second, at the proper operating conditions, the injector outputs too much fuel, causing the flame to extend significantly in the combustion chamber (Figure 3). This overheats the exhaust tube and is detrimental to the emission-analysis equipment mounted above the tube. Third, although the PERC system can accommodate the high pressure drop and volumetric flow rate necessary for this type of injector, the Delavan nozzle has exhibited operability issues in that it cokes – forms a carbonaceous solid when the fuel encounters a hot surface – when used, disabling the injector. This makes it more difficult to generate data with which to collaborate between the two laboratories.
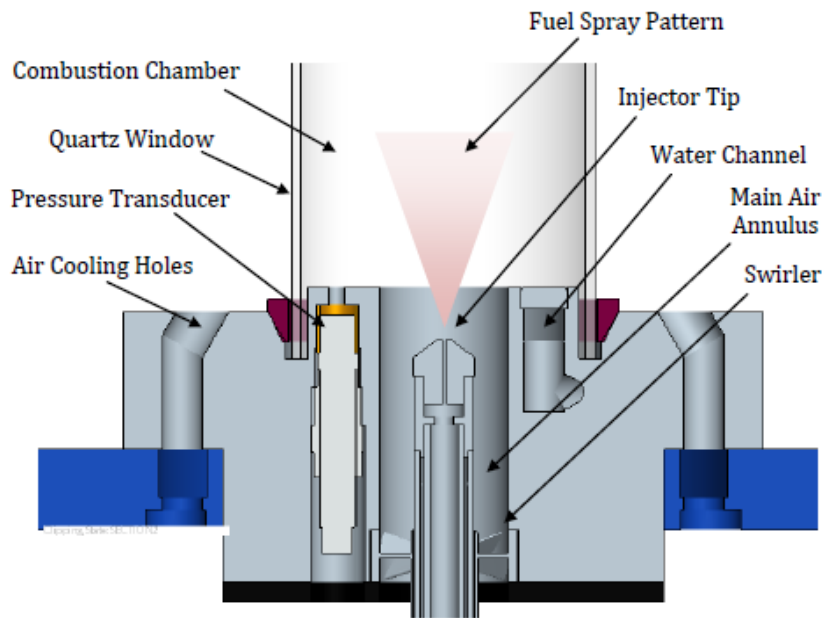
Figure 2. Cross-section of CRL atmospheric combustor using Delavan injector (adapted from [3]).

Figure 3. Flame extending past combustion chamber with Delavan injector
(adapted from [3]).

Fundamentals of Combustion

For combustion processes, the stoichiometric – or exact chemical quantity of oxidizer – mass air-fuel ratio is determined using

$$(A/F)_{stoic} = \frac{4.76\left(x+\frac{y}{4}\right)}{1}\frac{MW_{air}}{MW_{fuel}}. \tag{1}$$

Combustion frequently occurs under stoichiometric conditions; however, gas turbines typically operate at lower fuel flow rates to decrease the exhaust temperature and

pollutant emissions, specifically the amount of nitrogen oxide (NO and NO_2 are collectively referred to as NO_x) emissions. A parameter called the equivalence ratio

$$\Phi = \frac{(A/F)_{stoic}}{(A/F)}, \tag{2}$$

where A/F is the air-fuel ratio of the specific combustion process, is utilized to determine if a mixture is fuel lean − more oxidizer in combustion mixture than the stoichiometric amount − or rich − less than stoichiometric amount supplied to the mixture. The typical range for a gas turbine is approximately $\Phi = 0.6$-0.8.

The equation governing combustion of both gaseous and liquid hydrocarbon fuels is typically modeled in a simplified form using

$$C_xH_y + \frac{(x+y/4)}{\Phi}(O_2 + 3.76N_2) \rightarrow$$

$$bCO_2 + cCO + dH_2O + eH + fO_2 + 3.76\frac{(x+y/4)}{\Phi} N_2. \tag{3}$$
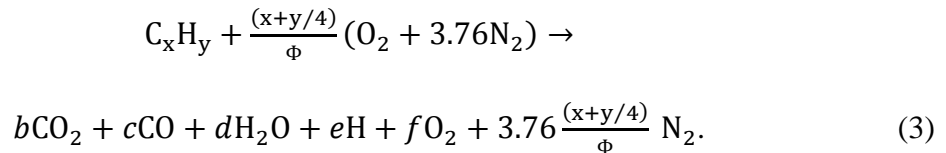
In Equation 1, it is assumed there is no dissociation of species. This equation can be employed when the stoichiometric amount − or exact chemical quantity − of oxidizer in the combustion process is utilized (so that $\Phi = 1$), or when any other amount of oxidizer is used.

Typically, combustion occurs in the form of a flame, a localized and self-sustaining zone which propagates at a subsonic velocity [5]. There are two types of flame structures in a combustion process: diffusion or premixed. In a diffusion flame, the fuel and oxidizing reactants are initially separated and combustion occurs at the interface

of the two, such as in a candle. Premixed flames are distinguished by a mixing of these two reactants at a molecular level before combustion, leading to a homogenous flame. The methane flame shown in Figure 1 is an example of a partially premixed flame with a gaseous fuel.

During combustion, it is important that the flame is positioned within a certain region in the combustor to minimize unexpected conditions within the combustion system, such as temperatures beyond the limit of a material. In the atmospheric combustor in the CRL, this region is made optically accessible by a quartz window (Figure 2) for flame-visualization studies. To ensure combustion occurs in this region, the system is designed so the flame anchors a certain distance from the injector tip. A flame is anchored when it is consistently located near a given point; a flame becomes lifted when it is no longer attached to that point.

Fundamentals of Atomization

The combustion of a liquid fuel – as well as its emissions [6] – is determined by the atomization of that fuel. Atomization is the process by which a set volume of fluid is dissipated into many small drops. These drops evaporate into a gaseous, combustible form. Atomization is controlled by several factors, such as fuel, oxidizer, and injector properties. The injector properties vary between the many different designs of injectors used today. One such property is the flow number, FN, defined as

$$FN = \frac{\dot{m}}{\sqrt{\Delta P \rho}}. \tag{4}$$

The flow number is a key parameter because it represents the effective area of the injector, so it is a gauge of the flow-path size. The flow number is often given in terms which are not dimensionally correct; however, the inclusion of a density term enables the expression to be used for a specific injector with various fluids [7].

When studying atomization, the key parameter is the droplet size. The goal is to design an injector which provides droplets within a range of 1 to 300 μm [7]. The time needed to evaporate and combust a droplet is directly related to the droplet's size, as shown by the D^2 Law

$$D^2(t) = D_0^2 - Kt. \tag{5}$$

Equation 5 can be utilized to determine the droplet lifetime, t_d, defined as

$$t_d = D_0^2/K. \tag{6}$$

The desired evaporation time is a function of the size of the combustor, impacting the amount of time the droplet will be within the combustion zone. One concern is that large droplets may pass through the flame zone and become unburned hydrocarbon, UHC, in the exhaust stream.

There is a distribution of droplet sizes in an atomization process. It would be difficult to perform calculations and analyses of a distribution, so average droplet diameters (see Figure 4) are often used. These average diameters are related by the volume fraction, Q. This parameter is the fraction of the volume of fluid in droplets smaller than the drop diameter, D. Although there are several different methods used to

determine average diameters, the Sauter mean diameter (SMD) is the most frequently

used in the literature. The SMD is the diameter at which the surface-to-volume ratio of

the droplet equals that of the spray, and it is considered to be more applicable to

combustion processes due to its relation to surface area and evaporation rates [8].
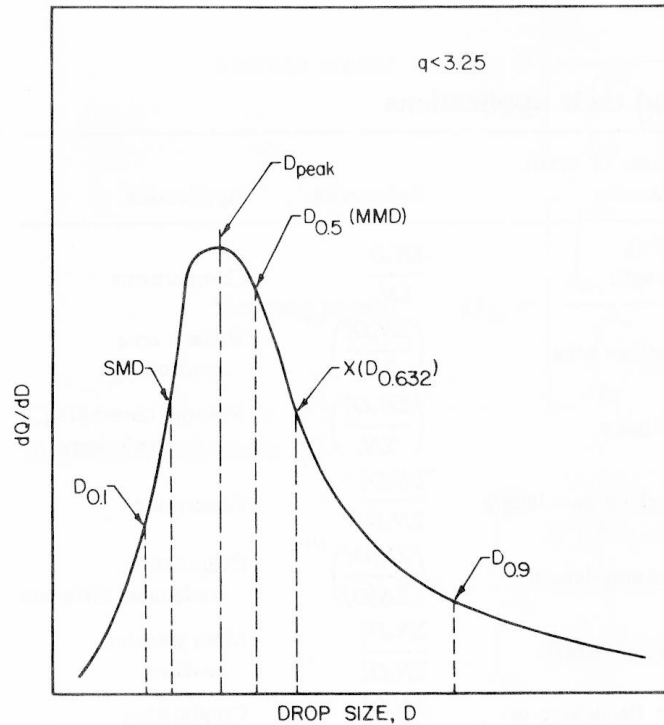
Figure 4. Droplet-size averages over spray distribution as a function of the volume
fraction, Q (adapted from [7]).

Various methods are employed to determine SMD and other mean-diameter

values for injectors through droplet collection or optical studies.

Direct-collection techniques rely on studying the droplets using a system inserted into the

flow, such as a slide into which the droplets impact. The droplets are very small, so they

have a short lifespan, especially after impinging on a surface. The short lifespan of these

droplets allows the dissipation of some of the injected fluid, decreasing the accuracy of the data. Many studies have been performed to determine novel ways of maintaining the drops for collection, including freezing the drops mid-flight with nitrogen or by mimicking liquid-fuel characteristics with media which would naturally solidify after injection [8].

Optical methods have the distinct advantage of not being greatly affected by significant droplet evaporation before data collection. The two methods typically used are through a light-scattering technique or through photographic imagery. The first process evaluates the light-intensity profile collected by a lens after passing through the flow. The second method relies on freezing the droplets in flight by using a strobe light. With a powerful burst from a strobe, a camera can utilize a high shutterspeed to stop the flow's motion. From these images, the droplet diameters can be measured. Some studies also employ double exposures to extrapolate droplet velocity. There have been recent advancements in methods which use laser or radio techniques for very small (0.3 to 3 μm) droplets [8].

Atomizer Types

The Delavan injector is a pressure-swirl atomizer. In this type of injector, high-pressure fuel is swirled before being emitted in a conical shape into the combustion chamber [7]. This style of injector is frequently used in diesel engines, jet-engine afterburners, ramjets, gas turbines, and industrial furnaces. Pressure-swirl injectors

usually require a high pressure upstream of the injector in the fuel line to operate, an issue in the CRL. The influence of injector pressure drop on SMD is shown in Figure 5.
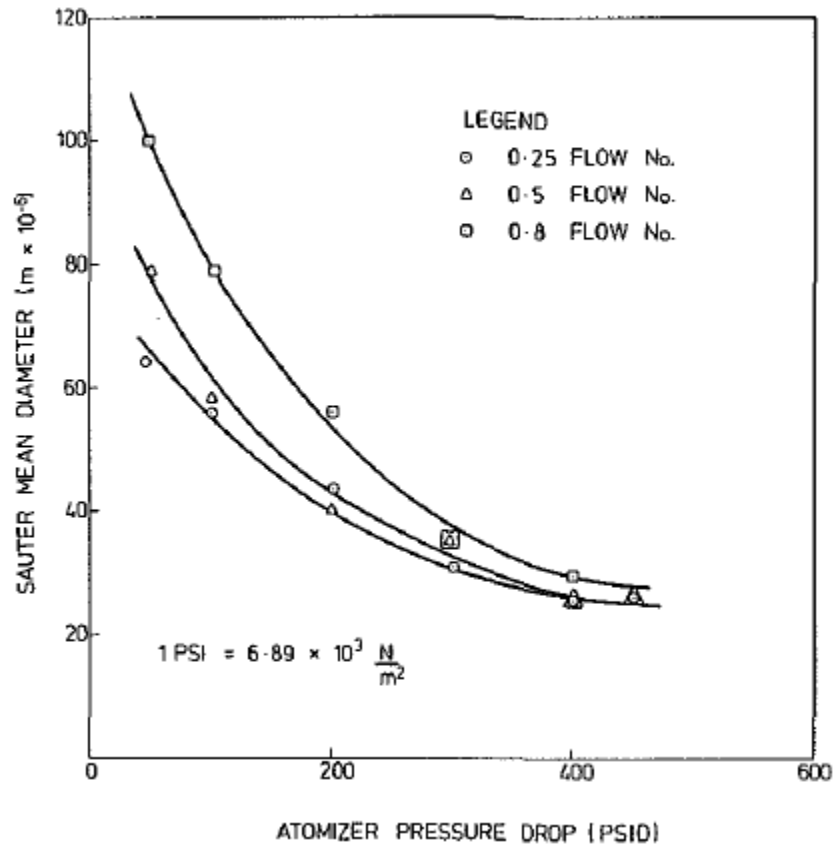
Figure 5. SMD as a function of pressure drop for the Delavan injector
(adapted from [6]).

Another study of pressure-swirl atomizer performance is shown in Figure 6. In this series of images, several different forms of injector patterns are demonstrated. The far left – called the "Dribble stage" and "Distorted pencil" – demonstrates the liquid jet in a beadlike form [8]. The "Onion stage" is generated when fluid velocity is increased further, until the stream is fully atomized into fine droplets [7]. The goal of an

atomizer would be to generate spray patterns in the "tulip" or, in the best case, the "fully developed spray" stages. With the Delavan injector, the best atomization will only occur with high pressures by design. This not acceptable at the CRL, so another injector style had to be used for the new atomizer.
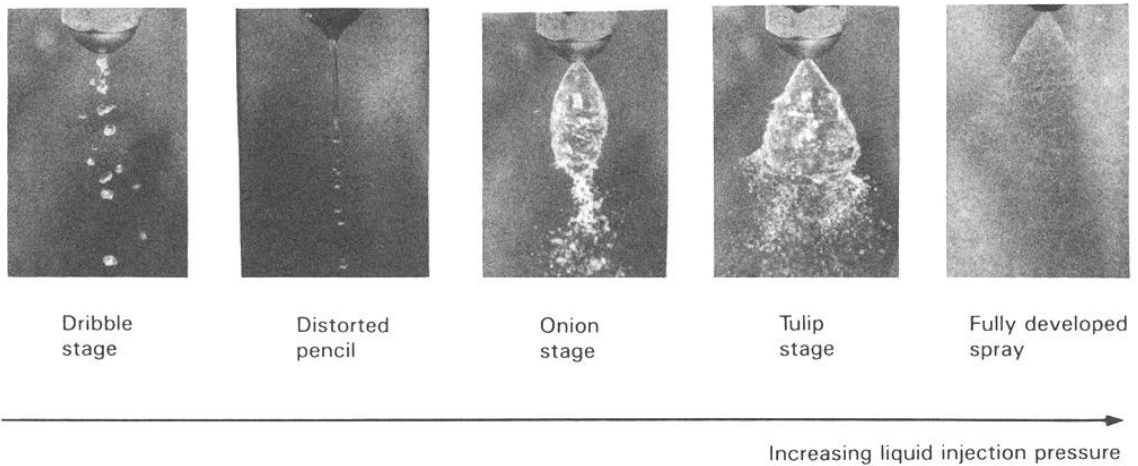
Figure 6. Images of progression of atomization stages with pressure using a pressure-swirl injector (adapted from [7]).

The pressure-swirl injector needs a high pressure drop across the injector to atomize because it does not have a secondary fluid flow to disperse the fuel flow. When liquid is injected in the absence of a secondary atomizing fluid flow and at a lower pressure than typically used in a pressure-swirl injector, the droplet size can be approximated by using the idealized Rayleigh mechanism of breakup. This theory estimates each droplet diameter, D, to be sized according to

$$D = 1.89d. \tag{7}$$

Figure 7 shows a model flow using this theory, as well as an experimental breakup of droplets. The experimental distribution is similar to that demonstrated by the prototype test section used in this study, shown in Figure 8, operating without atomization air.
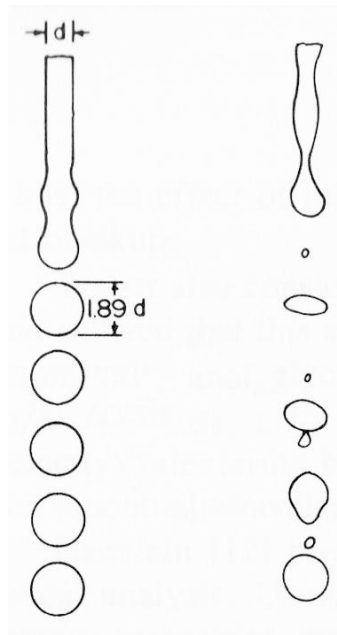
Figure 7. Idealized jet breakup according to Rayleigh mechanism (left) and in experimental study (right) (adapted from [7]).

Figure 8. Example of jet breakup using test system.

New Injector Style Determination

The new injector was designed with a secondary fluid flow to aid in the atomization process. The chosen alternative style is an airblast atomizer. Airblast atomizers are a type of injector in which the fuel flow is sheared using large amounts of air at low flow rates. These injectors require a lower fuel pressure, and generate a finer fuel spray, which creates lower amounts of soot and exhaust smoke than that generated by pressure injectors during combustion because of a complete mixing of fuel and air [9]. Airblast injectors also demonstrate a constant distribution of droplet sizes over all flow rates [10].

The mechanics behind airblast atomization are basic. Viscosity – the force demonstrated as an internal cohesive force in liquids [11] – opposes the transition of the liquid ligaments into droplets, resistance which continues even as the droplets continue to atomize into smaller forms. Surface tension – the action of a droplet to hold together as if it has a membrane [11] – delays the initial formation of the ligaments during the atomization process [8]. Fluid develops into ligaments, then large droplets, and then smaller, atomized droplets. The disintegration of the ligaments is caused by waves generated by the surrounding air which cause the instabilities necessary for atomization of the flow [8].

A plain-jet airblast atomizer has a very simple design because it injects the fuel into the high-velocity air as a discrete jet [7]. The goal is to create a jet of fuel which is surrounded by a coaxial coflow of air [8]. Even with a simple design, plain-jet airblast

atomizers demonstrate a good range of SMDs as a function of pressure drop, as shown by Figure 9.
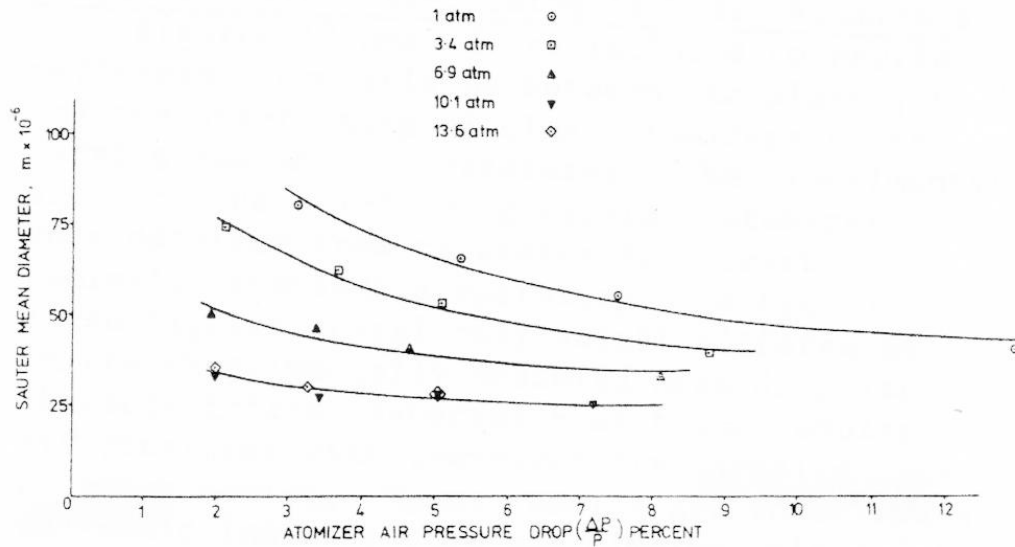
Figure 9. SMD as a function of pressure drop for a representative plain-jet airblast atomizer (adapted from [9]).

Several configurations of converging plain-jet airblast atomizers were used as guides for the design of the CRL's new injector [8]. The first is the Nukiyama-Tanasawa atomizer, shown on the left side of Figure 10. This model represented the first significant investigation of airblast atomization [7]. The second model is the Lorenzetto-Lefebvre injector, shown on the right side of Figure 10. Data from the testing of the Lorenzetto-Lefebvre injector demonstrated decent atomization characteristics [7,10]. This style was chosen due to its particularly simple design, the ability to alter geometry after initial design and manufacture, and the injector's ease of disassembly, allowing cleaning – a factor absent in the Delavan injector.
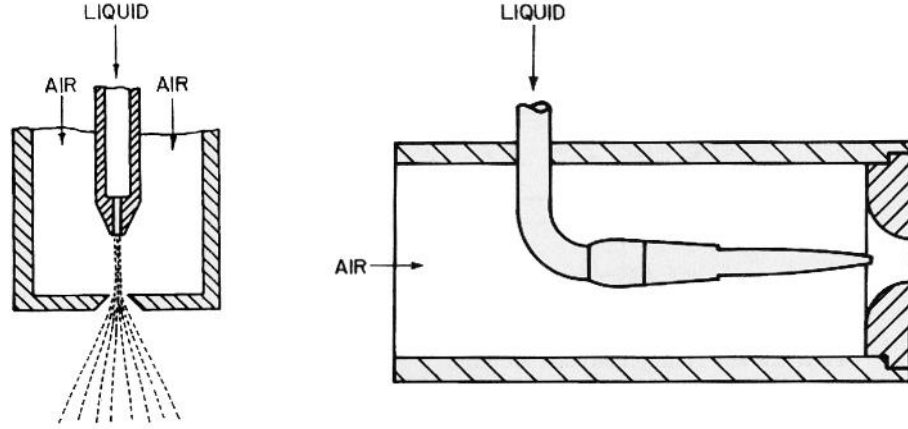
Figure 10. Nukiyama-Tanasawa plain-jet airblast atomizer (left) and Lorenzetto-Lefebvre plain-jet airblast atomizer (right) (adapted from [8]).

In the Nukiyama-Tanasawa study, a correlation was created to evaluate experimental SMD results and curve-fit these data using physical parameters upon which airblast atomization operates, such as density, surface tension, and relative velocity. This resulting correlation, however, does not take geometry effects into account:

$$\text{SMD} = \frac{0.585}{U_R}\left(\frac{\sigma_L}{\rho_L}\right)^{0.5} + 53\left(\frac{\mu_L^2}{\sigma_L\rho_L}\right)^{0.225}\left(\frac{Q_L}{Q_A}\right)^{1.5}, \tag{8}$$

where: U_R is the velocity of the air relative to the liquid,
σ_L is the surface tension of the liquid,
ρ_L is the density of the liquid,
μ_L is the dynamic viscosity of the liquid,
Q_L is the volumetric flow rate of the liquid, and
Q_A is the volumetric flow rate of the air.

Although the new fuel injector design will be discussed later in this document, it is important to note here that the final design most closely resembles the Nukiyama-

Tanasawa injector configuration. Therefore, it is extremely valuable to have information which will relate the geometrical parameters of this injector to the flow characteristics.

Numerous studies indicated that injector geometry was unimportant; however, it was deemed necessary to properly investigate this claim in the design of the new injector. O'Shaughnessy *et al.* [12] did determine that the geometry within the injector – specifically the jet breakup mechanism – played a role in the atomization process. The key dimensions of the plain-jet airblast atomizer utilized in their study are shown in Figure 11. The key dimensions as defined in Figure 11 are: the injector distance between the exit of the fuel orifice and the exit of the injector, h; the diameter of the injector exit orifice, d_a; and the diameter of the fuel orifice, d_F [12].
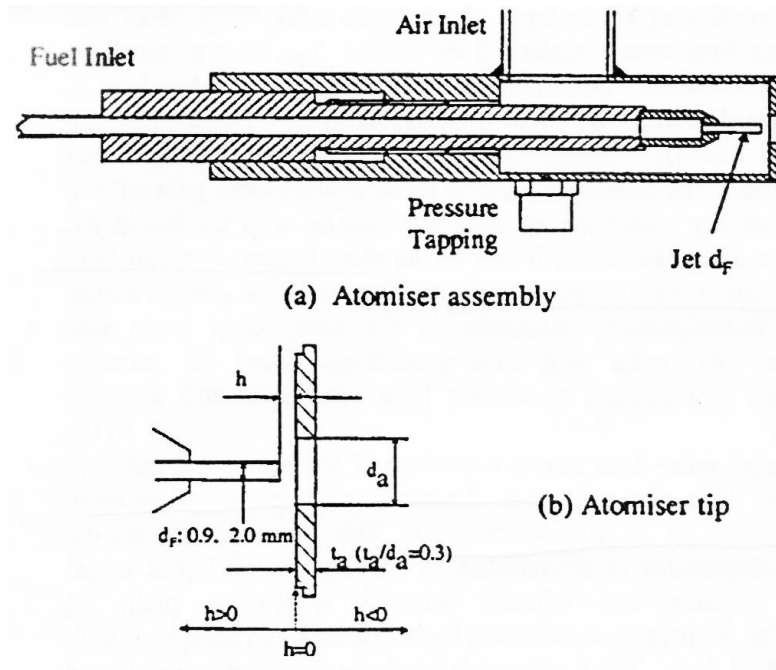
Figure 11. Schematics of O'Shaughnessy *et al.* plain-jet atomizer representative dimensions (adapted from [12]).

The impact of variance in these parameters – as well as the air/fuel ratio (AFR) – on measured SMD values is shown in Figure 12. The study demonstrated that when injector distance, h, is greater than zero, SMD increases; when h is less than one, SMD is the same as when the fuel jet is in line with the orifice (h = 0) [12]. The impact of increasing air flow velocity is also evident.

Figure 12. SMD as a function of injector parameters (adapted from [12]).

The O'Shaughnessy *et al.* study aimed to utilize the Nukiyama-Tanasawa correlation (Equation 8) and modify it to include geometry data specific to a certain injector. By evaluating experimental data for several injectors and correlating the data with the Nukiyama-Tanasawa equation, the authors developed the following correlation for SMD:

$$\text{SMD} = C_1 \frac{3}{\left[\frac{2}{d_F} + \frac{C_2 \rho_L U_A^{1.5}}{4\sigma_L(1+1/\text{AFR})}\right]},$$ (9)

where: C_1 and C_2 are constants,

   d_F is the diameter of the liquid flow, and

   U_A is the air velocity.

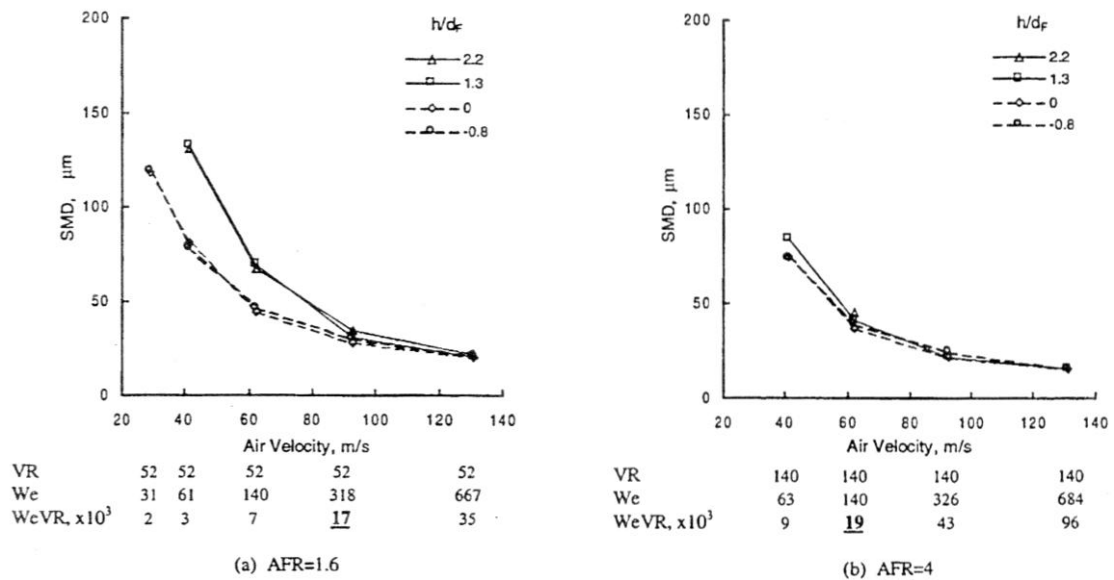Since O'Shaughnessy *et al.* utilized the correlation they developed and curve-fit experimental data considering the geometric parameters of the Nukiyama-Tanasawa injector, the two correlations (Equation 8 and Equation 9) should predict the same SMD, within acceptable experimental uncertainty. Therefore, the equation can be utilized for a specific injector by plotting experimental results together and determining values of C_1 and C_2 for which the two correlations estimate similar results. This is the method that will be used later in this study to provide quantitative analysis of the experimental results obtained from the prototype testing.

EXPERIMENTAL DESIGN

   The basic configuration of the new injector design allows for easy changes in the injector's geometry, particularly the injector distance, h, of the fuel outlet from the exit orifice of the atomizer. Changing this parameter on the new injector requires the creation of another injector cap and demonstrates significant changes in the spray characteristics, as discussed earlier. The conditions of the flow – such as spray pattern– are very difficult to determine while inside of the combustor, but it is important to examine visually how

the system reacts at different flow rates before a flammable fluid is used. To accomplish this, a prototype injector was tested with water in a spray delivery and collection system.

To ensure that data were collected for test conditions similar to those utilized in the CRL, nominal flow rates of a representative hydrocarbon liquid fuel, heptane, were calculated at the maximum air flow rate of 184.1 SLPM (see Table 1). Additionally, as is standard practice in combustors, the air flow rates required for the atomization process were calculated as a percentage of the main air flow rate (see Table 2).

Table 1. CRL fuel flow rate test conditions for heptane.

Φ	Volumetric Flow Rate (CCM)
0.5	7.78
0.6	9.34
0.7	10.90
0.8	12.45
0.9	14.01
1.0	15.56

Table 2. CRL air flow rate test conditions.

Percentage of System Air	Volumetric Flow Rate (SLPM)
5.0	9.21
6.0	11.05
7.0	12.89
8.0	14.73
9.0	16.57
10.0	18.41

The prototype test system is similar to what was used by O'Shaughnessy *et al.*, shown in Figure 11. Air and fuel flow rates were varied, as well as the injector distance. The outer orifice diameter (d_a in Figure 11) was not altered since it was shown that this

dimension did not have a noticeable impact on atomization characteristics for low-viscosity fluids [8,12]. It is standard practice to use water for these tests; the use of water instead of heptane should not negatively impact the results of the tests because liquid density and viscosity do not have a significant effect on atomization, and, moreover, these two liquids have relatively similar properties. Water's slightly higher density could affect atomization such that higher SMDs are generated than if the tests were run with heptane, but this would simply make the injector generate even better patterns when used [8]. A photograph of the test system is shown in Figure 13, and Figure 14 is a schematic of the final design.
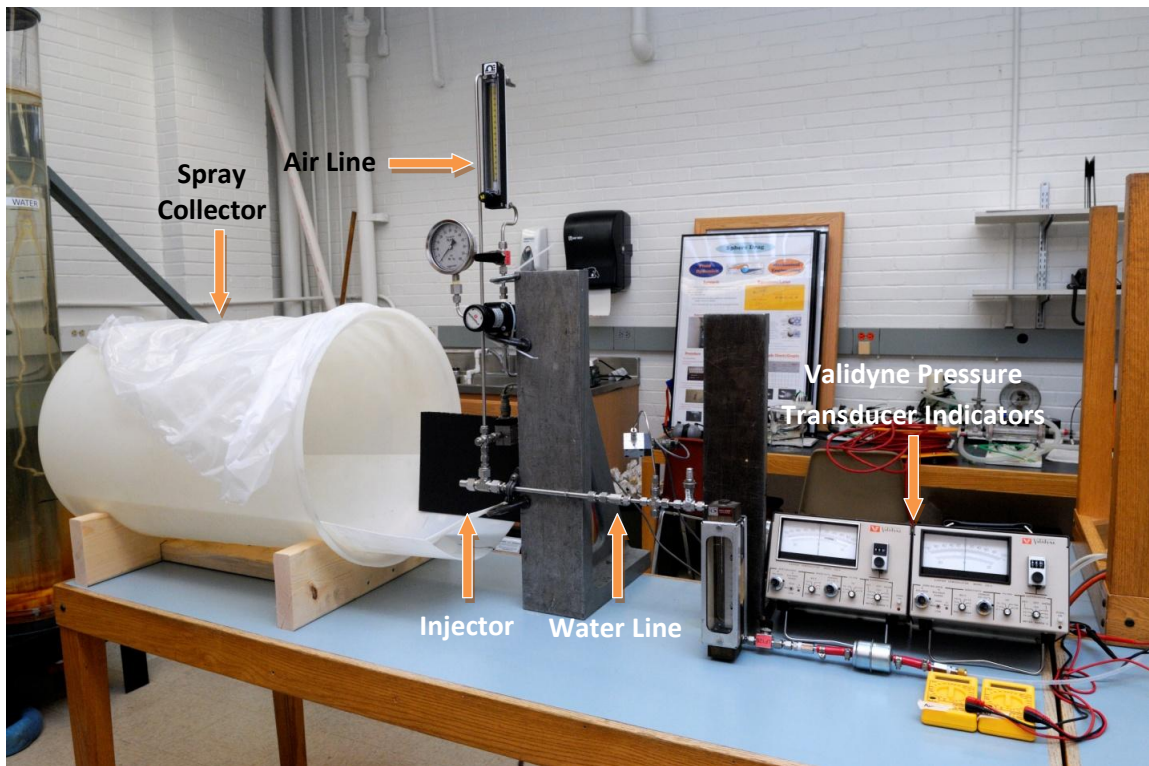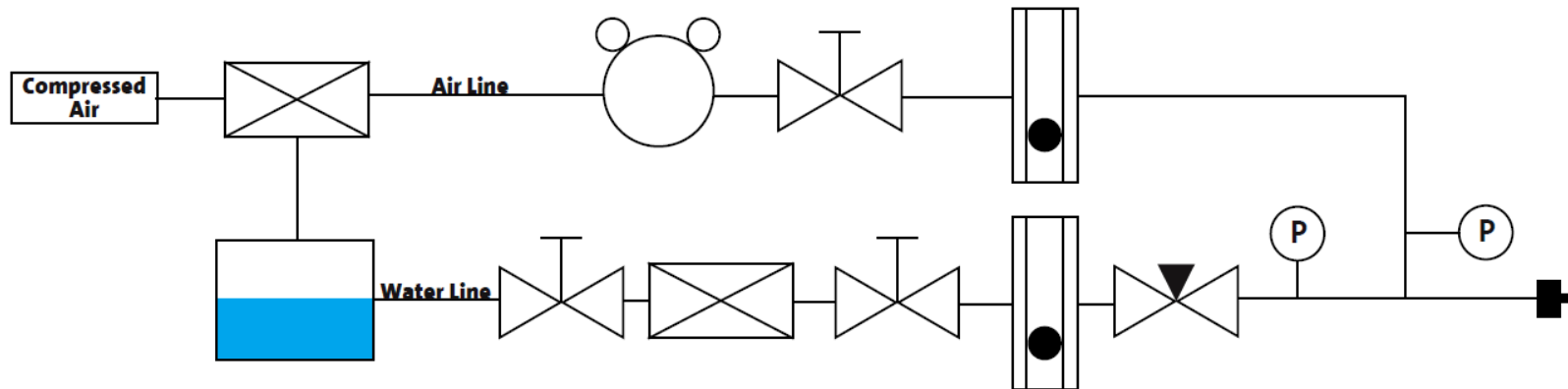

Figure 13. Photograph of test system.

Figure 14. Test system schematic.

Injector Tester Design

The test system was designed to take advantage of available materials from the CRL to minimize cost and construction time. The exit-orifice end of the test section is shown in Figure 15. The system employs a tube-in-tube design in which the inner, water-line tube is 0.375 inches, and the outer, air-line tube is 0.5 inches. These components are typically used in the CRL as the liquid-fuel line.
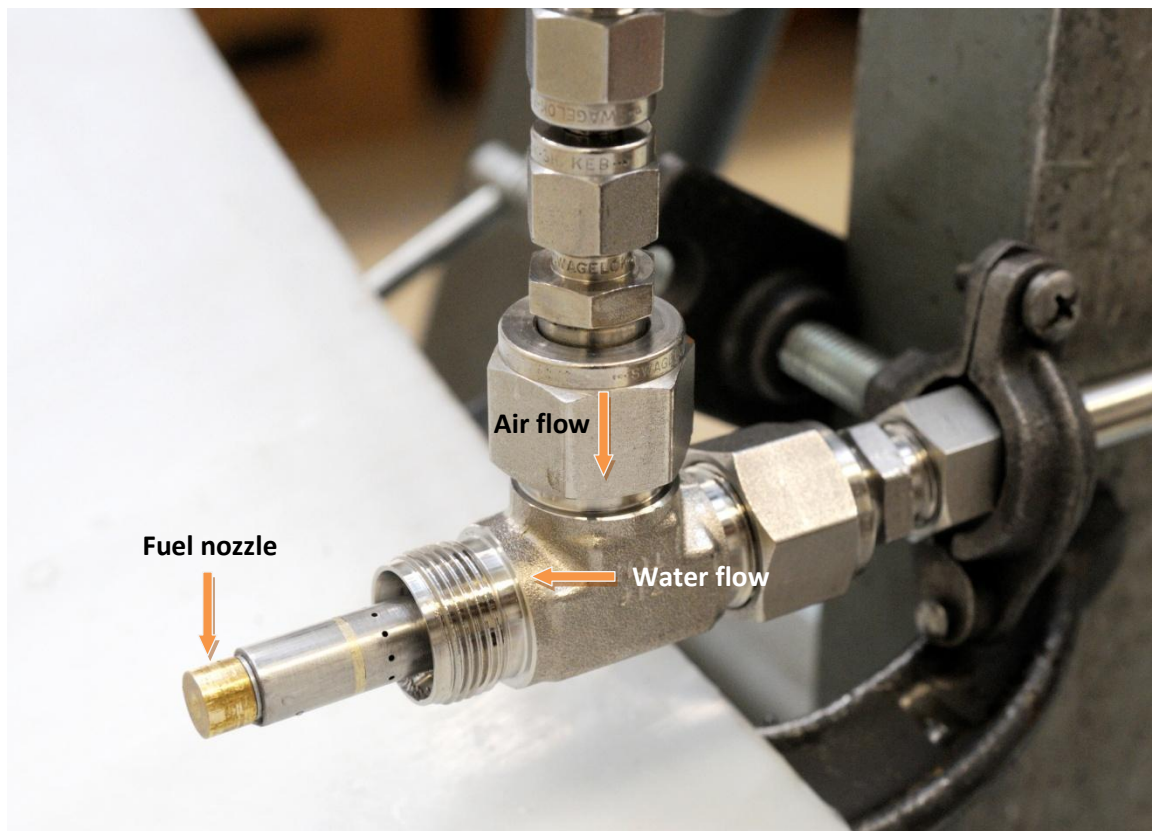
Figure 15. Exit-orifice end of the test system.

Water Line

Two nozzles were supplied for use as the fuel-line injector. The diameter (d_F in Figure 11) of each, however, was not known precisely. This dimension is key to evaluate

the fuel flow rate – thereby the equivalence ratio, flow number, and many other properties – through the injector. To determine the diameter, each was viewed in a scanning electron microscope (SEM), and it was determined that there were two relative sizes, shown in Figure 16 (injector #1) and Figure 17 (injector #2).

Figure 16. SEM image of nozzle #1.
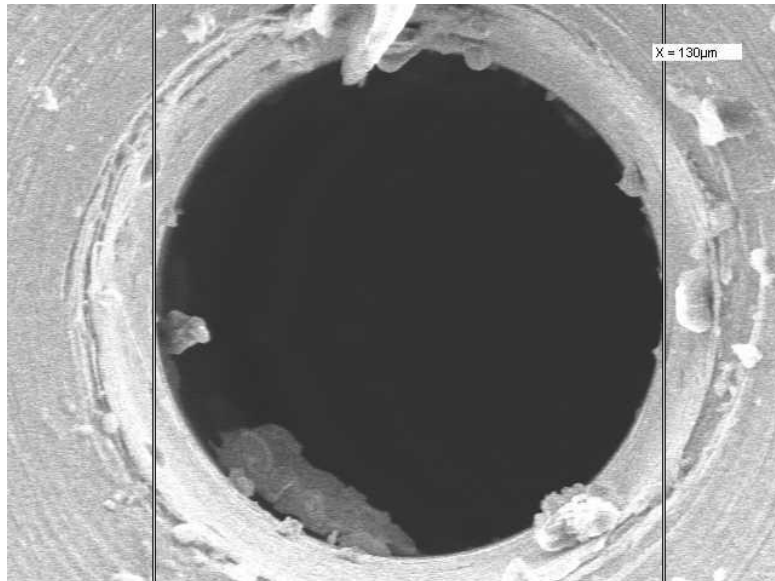
Figure 17. SEM image of nozzle #2.

In the test system, water was supplied from a one-gallon pressure vessel. It flowed through Federated Auto Parts GF68 automotive gas-line filter and into a rotameter. The filter was deemed necessary because of concerns of 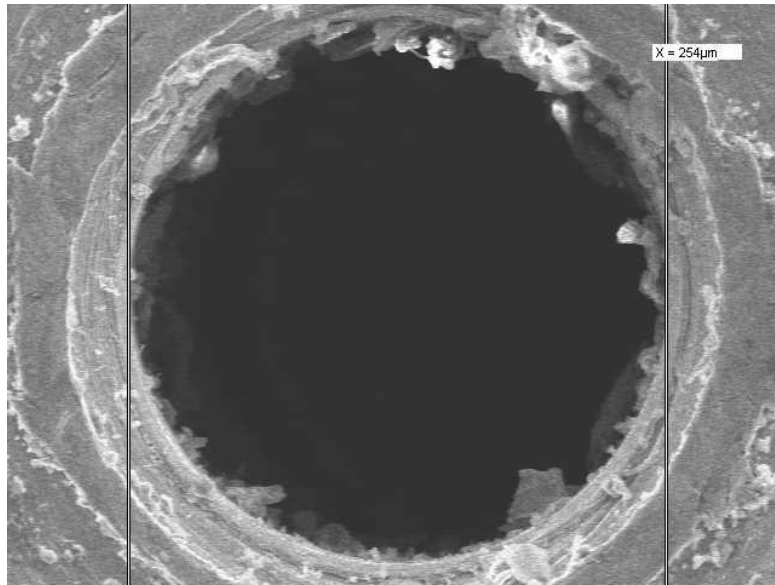rust and other particulates damaging the system. A Swagelok SS-4MG Medium-Flow Metering Valve was used to control the water flow rate and was placed downstream of the rotameter to minimize the likelihood of cavitation, a phenomenon during which variances in pressure generate vapor bubbles [11].

A Brooks 2-1110-6 rotameter with a Brooks R-2-15-D tube was used to measure the volumetric flow rate of the water. A calibration of this rotameter is shown in Figure 18.

Figure 18. Volumetric flow rate as a function of float height with Brooks 2-1110-6.

A series of tests with nozzles #1 and #2 was performed, and it was determined that the flow rates through nozzle #1 were too high for use at the CRL but may be

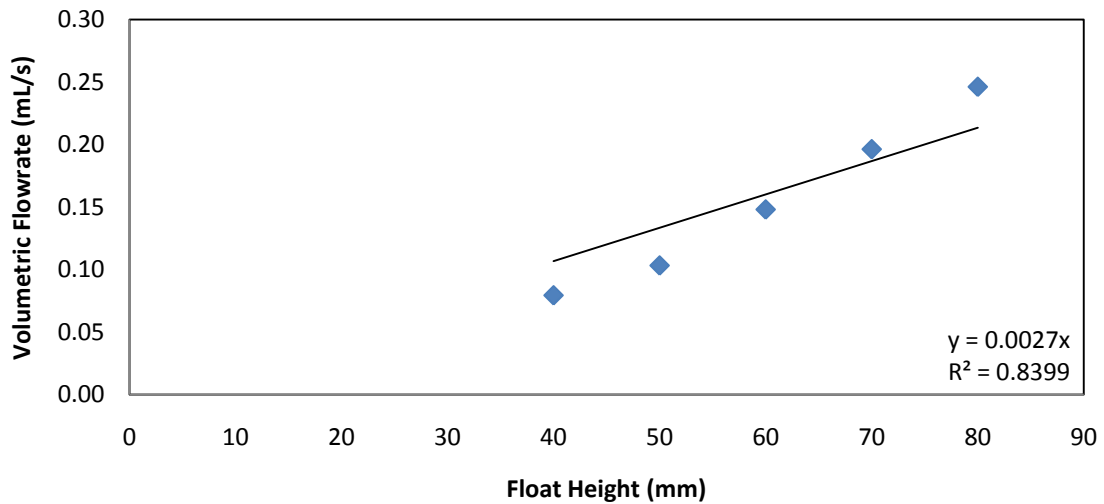representative of the flow used at PERC. Flow rates through nozzle #2 were similar to those utilized at the CRL (see Table 1), so it was used for the remainder of the tests.

Air Line

A Craftsman 160 psi 1.6 hp compressor was used to supply air to the system. The compressor was connected to a Motor Guard Model M-30 Compressed Air Filter which linked with a splitter to pressurize the water tank and the atomization air line. The flow was regulated to 45 psi with a Fairchild Model 1000 Precision Pressure regulator equipped with an Ashcroft 60 psi gauge.

An Omega FL-3439ST-VN rotameter was utilized to measure the volumetric flow rate. A calibration performed by Omega for this rotameter is shown in Figure 19. The air-line system on the test apparatus is shown in Figure 20.
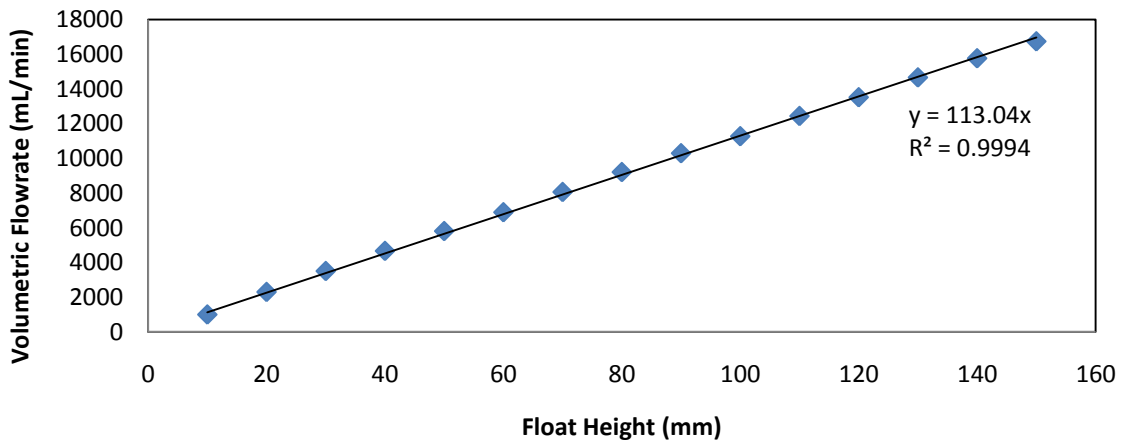
Figure 19. Volumetric flow rate as a function of float height with Omega FL-3439ST-VN from Omega-performed calibration (data from [13]).
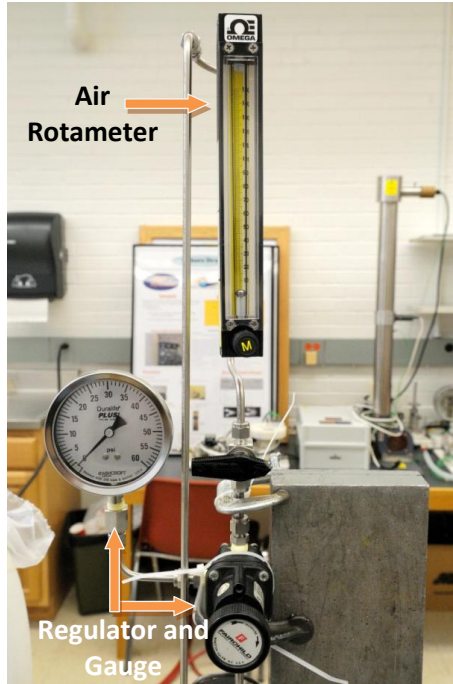
Figure 20. Air-line system on test apparatus.

Pressure Measurement

Both the air and fuel lines needed pressure measurements to calculate the pressure drop across the injector, a key goal of this project. Two Validyne CD12 Transducer Indicators were used to evaluate the signal from the pressure transducer units on the water and air lines, both of which used 80 psi diaphragms. The voltage outputs from the transducer indicators were connected to two Cen-Tech P30756 digital-display multimeters. The indicators and multimeters are shown in Figure 21, and the pressure transducer on the air line is shown in Figure 22. The transducers were calibrated with an Armfield Portable Deadweight Gauge Tester. The voltage-pressure correlation is

$$\frac{V}{10} = \frac{X_P}{80}. \tag{10}$$
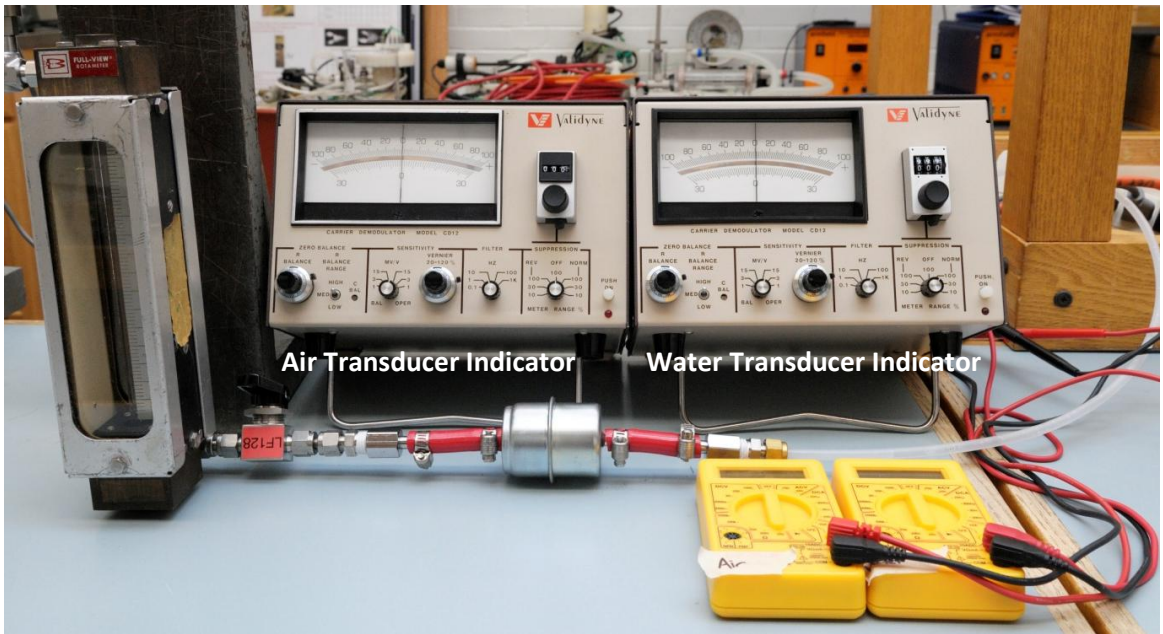
Figure 21. Pressure transducer indicators and multimeters.

Figure 22. Air-line pressure transducer.

Variance in Orifice Spacing

The injector distance, h, was adjusted by moving a 0.5-inch cap. To measure the injector distance, a Size 60 drill bit − the same size as the 0.040-inch orifice − was inserted until it stopped at the front of the nozzle. The depth was marked with a piece of tape (Figure 23) and then measured with calipers.   This setup was very easy to manipulate, allowing a range of test points.   It did not, however, enable specific test points to be chosen (i.e. 0.040, 0.140, and 0.240 inches were impossible to select exactly).

Figure 23. Example of depth measurement.

Data Acquisition

The simplest of the myriad ways to study the atomization ability of an injector optically is with a camera. For this study, a Nikon D300 with a Nikkor 50mm f/1.8D AF mounted on a tripod level with the exit orifice of the injector was used. The exposure was manually set to f/11 and 1/250 s at ISO 560. The test employed Nikon's 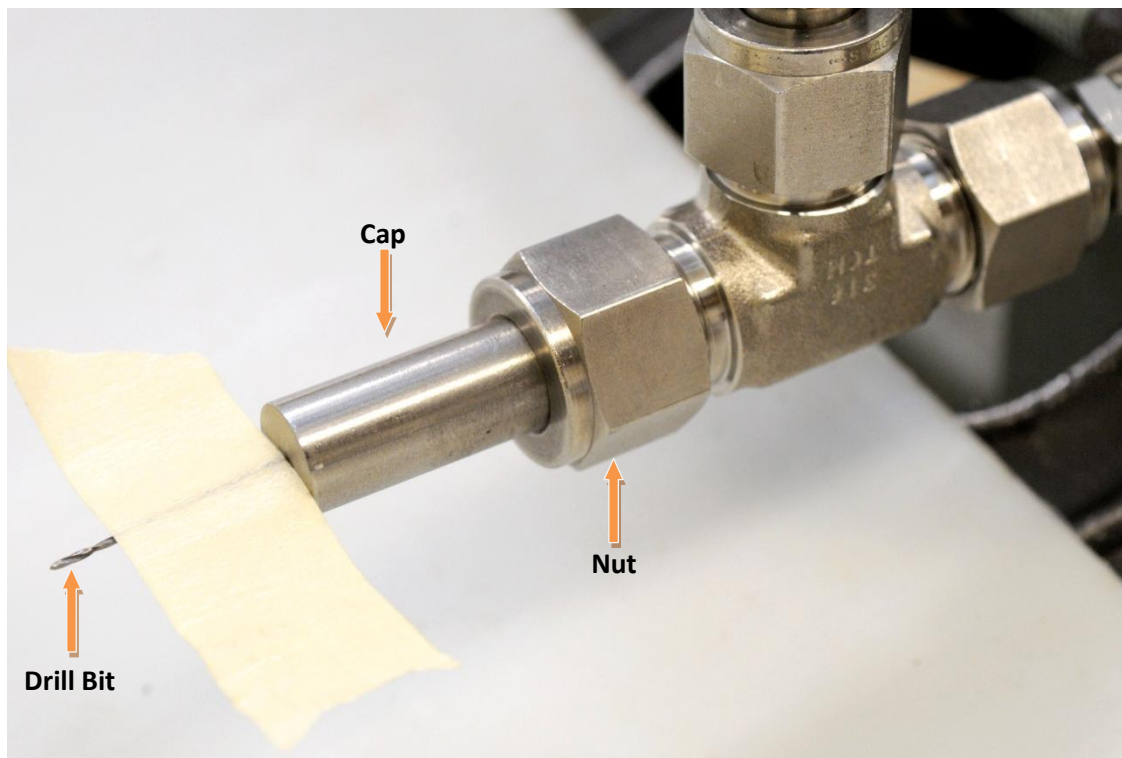Creative Lighting System (CLS) with a Nikon SB-900 held above the injector in Remote mode and the D300 in Commander mode. The on-camera flash was set to zero, and the SB-900 was manually set to 1/100 intensity and 70 mm. The lens was focused in continuous autofocus mode, and then locked in manual mode to maintain the same depth of field in all tests. The D300 was remotely fired with a Nikon MC-36 to minimize disruption of the camera.

PROCEDURE

Spray patterns over a range of injector distances and flow rates were collected. The test points were determined by calculating the volumetric flow rate of heptane over a range of equivalence ratios (Table 1) and the flow rate of atomization air as a percentage of maximum air flow rate (Table 2) in the CRL. First, the injector distance was measured by the method described earlier. To ensure the water jet and exit orifice remained coaxial, the water was left on during the tightening of the nut. Next, the water flow rate was first set at a height of 70 mm on the Brooks rotameter, and the pressure in the water line was recorded. Increased resistance would cause the water flow rate and pressure values to change when the air line was activated, so the procedure required acquiring the

water values first. The air line was opened and first set to a height of 80 mm on the Omega rotameter. The voltage from the air-line transducer was recorded, and a photograph was taken with the D300. This process was repeated for water flow rates 30-70 mm (4.248-14.568 CCM) in increments of 10 mm and air flow rates of 80-140 mm (4.91-8.55 percent of CRL air) in increments of 20 mm for a total of 20 test points per injector distance (h = 0.041, 0.137, or 0.240 inches). Once this matrix of points was obtained, another data set would be collected for a new injector distance. This process was developed to provide sufficient coverage of physical test conditions without requiring an unmanageable number of test points. Additionally, performing the data collection in a uniform manner ensured that results at similar conditions could be compared directly.

RESULTS AND DISCUSSION

Approximately 180 data points were collected from the test system at various flow rates and injector distances. These included 17 test points at 4 injector distances (h values) which were recorded with the larger diameter (nozzle #1, shown in Figure 16), and 161 test points at 15 injector distances recorded with the diameter sized for the CRL (nozzle #2, shown in Figure 17). The flow conditions could not be reached for some of these planned data points due to the pressure issues discussed later in this document.

The flow number of the new injector was calculated to be $1.33 \cdot 10^{-8}$ m^2, whereas the flow number of the Delavan injector is calculated to be $2.02 \cdot 10^{-8}$ m^2 [3]. This demonstrates that the new design achieves the goal of a smaller effective flow area.

The maximum pressure drop for the liquid across the injector in the test system was 40 psid, significantly less than the 110 psid drop experienced with the Delevan injector in the previous work [3].

Photographic Results of Testing

For each test point, an image was taken of the flow pattern. Using those images, the effect of injector distance, h, between the fuel orifice and the exit orifice of the injector can be first demonstrated with the three images shown in Figure 24.

Injector Distance: 0.041 in.

Injector Distance: 0.137 in.

Injector Distance: 0.240 in.

Figure 24. Spray-pattern images for a range of injector distances at 9.41 CCM water and 15.78 LPM air.

Figure 24 demonstrates a fully developed spray for each injector distance. It also shows that, as the injector distance is decreased, the spray pattern moves closer to the orifice of the injector. The atomizer appears to generate the desired atomization at all injector distances, so the movement of the spray pattern is the aspect which will most impact the final design. The combustion environment in which this injector will be used

will consume the droplets shown on the left-most side of the frames in Figure 24, so the right side should be relatively consistent. By placing the spray pattern closer to the injector tip, the likelihood that more fuel will be vaporized and combusted after atomization increases.

Another parameter studied for injector design is the spread angle of the spray from the centerline. This angle is important because if it is too obtuse, the spray will be too wide for the combustion system and droplets could impinge upon the surface of the quartz window, potentially leading to combustion on that surface. Figure 24 does not, however, appear to show any relationship between injector distance and the spray's spread at its widest point.

The impact of the variance in air/fuel ratio (AFR) with a constant water flow rate is demonstrated in the series of photographs in Figure 25. Droplet size decreases from the large droplets are shown in the top-most image of Figure 25 to smaller drops as AFR increases.

Air: 9.07 LPM

Air: 11.31 LPM

Air: 13.54 LPM

Air: 15.78 LPM

Figure 25. Series of photographs at water flow rate of 12.00 CCM and h = 0.137 in.

A region of interest as defined by Figure 26 was chosen. To better show the impact of increasing air flow rate, Figure 27 was created from high-resolution sections of the center of the atomized flow from this defined region. The camera was unable to fully freeze the flow, but it is relatively easy to see the progression from the larger droplets at 9.07 LPM of air to the finer mist created by the 15.78 LPM of air condition.
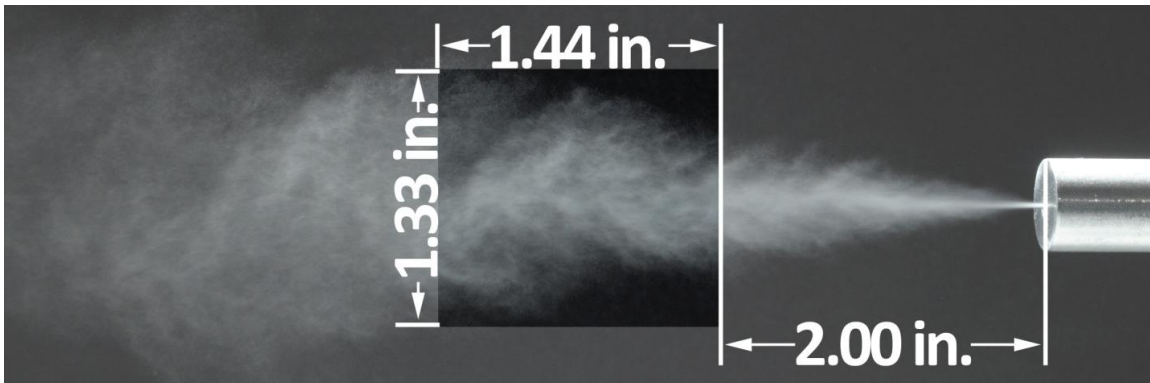

Figure 26. Scale used for high-resolution sections from 15.78 LPM flow condition image.
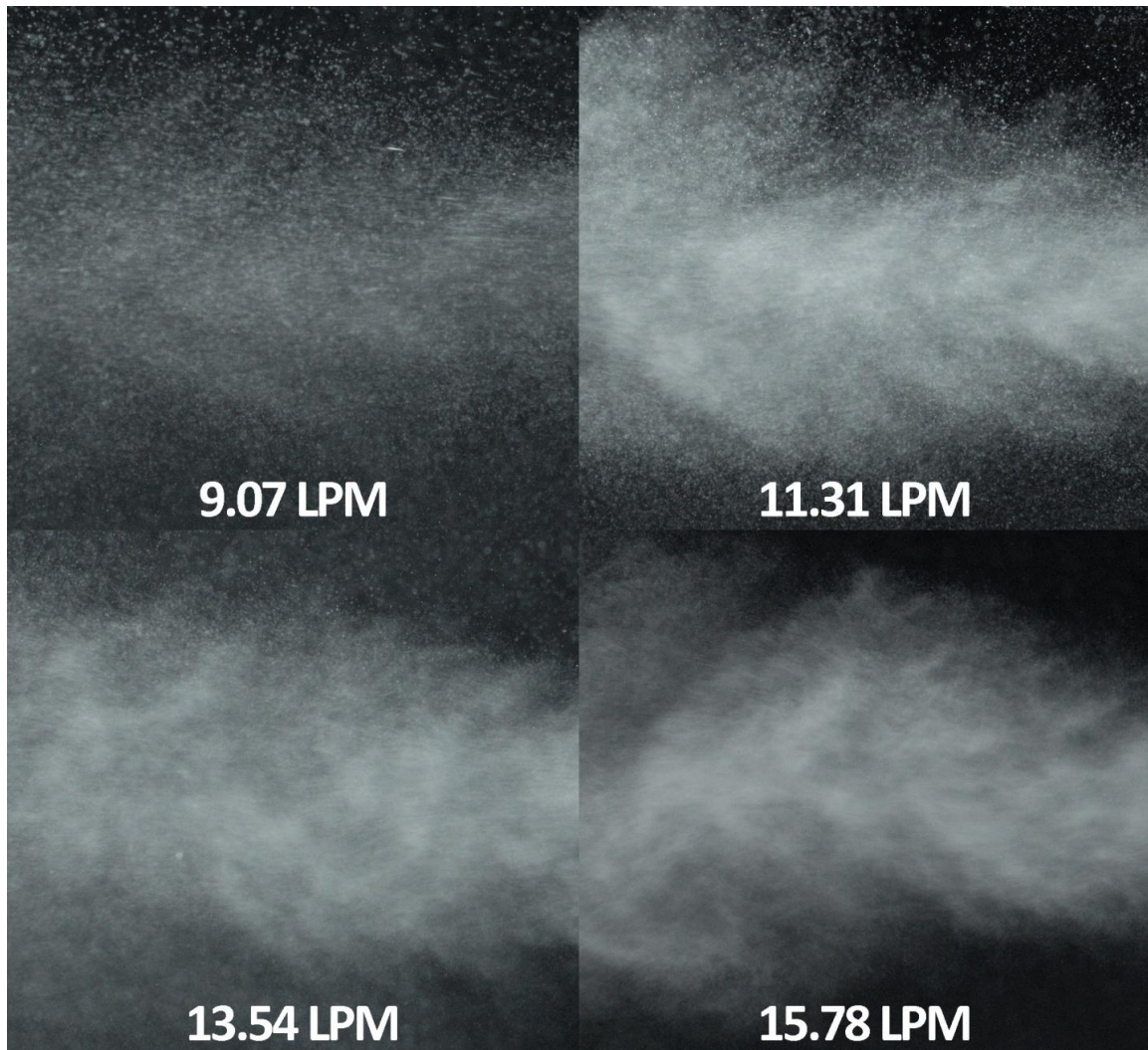
Figure 27. Series of cropped photographs of the center of the atomized flow at a constant water flow rate of 12.00 CCM and injector distance of 0.137 in.

SMD Estimation from Experimental Correlations

Whereas the images demonstrate qualitative results, quantitative analysis of the effectiveness of this new injector concept was also made. Figure 28 demonstrates the impact of air velocity on SMD using Nukiyama-Tanasawa correlation, Equation 8.
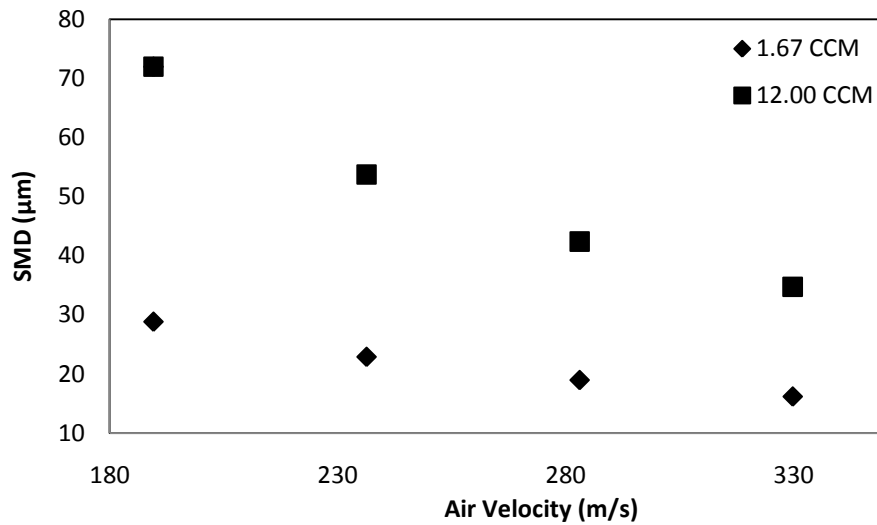
Figure 28. SMD as a function of air velocity using Nukiyama-Tanasawa correlation with 1.67 and 12.00 CCM water and h = 0.041 inches.

Since Equation 8 does not incorporate injector geometry into estimating SMD, all of the data points for each injector distance would provide the same value. This figure demonstrates what was shown qualitatively in Figure 25 and Figure 27: As air flow rate or air velocity is increased, the SMD decreases, independent of water flow rate.

As discussed earlier, O'Shaughnessy *et al.* introduced Equation 9 as a correlation to estimate SMDs with geometry effects included. No means by which SMD could be experimentally determined was available for this study, so a comparison between the results of Equation 8 and Equation 9 was utilized. This is a valid approach because both correlations should result in approximately the same value; the key is determining the values of C_1 and C_2 which generate the SMD results with the best accuracy. The comparisons are shown in Figure 29, Figure 30, and Figure 31 for the measured injector distances of 0.041, 0.137, and 0.240 inches, respectively. In each figure, the

values of C_1 and C_2 were optimized to create the best fit (determined by maximizing R^2 value).
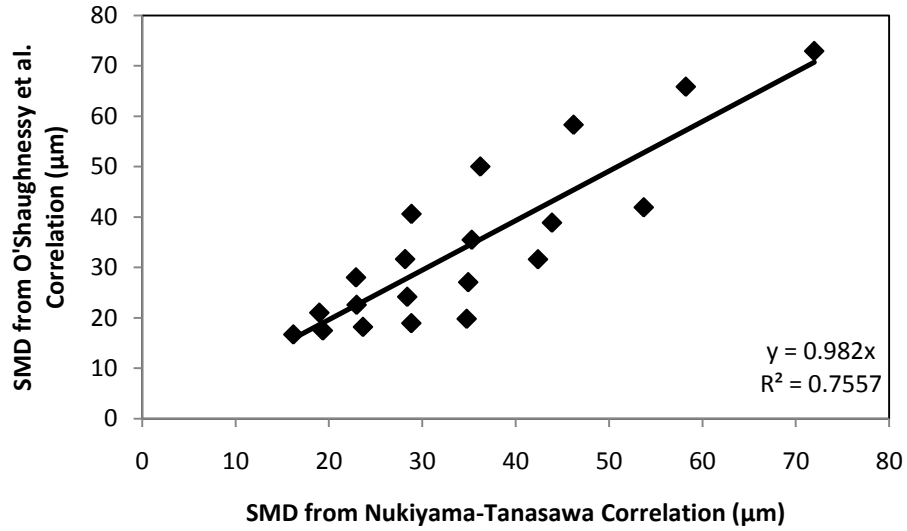

Figure 29. SMD comparison for 0.041 in. using $C_1 = 1.0500$ and $C_2 = 0.0087$.
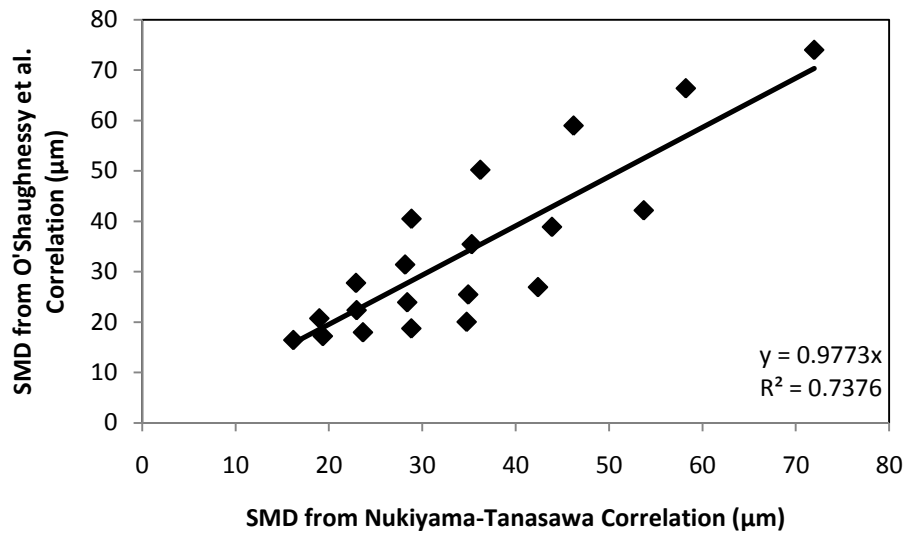

Figure 30. SMD comparison for 0.137 in. using $C_1 = 1.1000$ and $C_2 = 0.0093$.
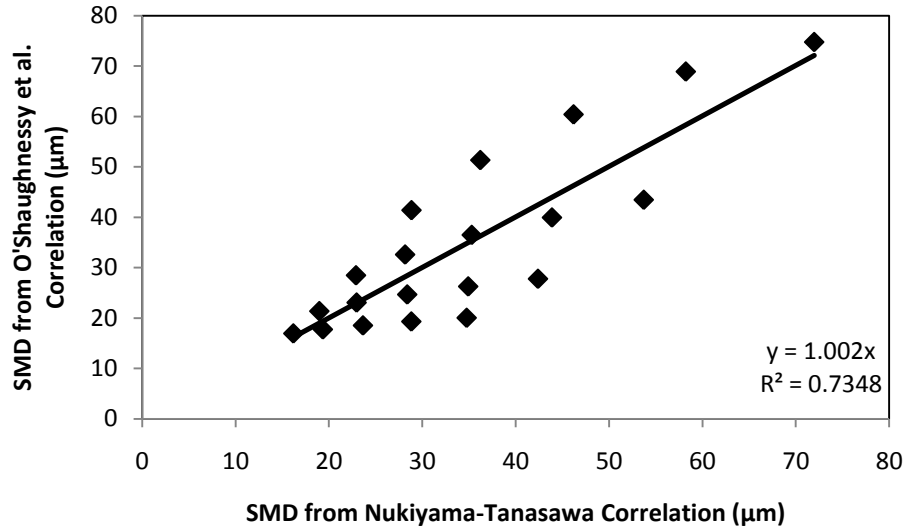
Figure 31. SMD comparison for 0.240 in. using $C_1 = 1.1000$ and $C_2 = 0.0090$.

It is apparent that the R^2 value for each data set shown above is low; however, this is because each trendline is fit with the assumption that the data are forming a scatterplot, which is not correct. In reality, the data presented in these figures have distinct trends associated with the water flow rate values. This is shown more clearly in Figure 32, where the data have been separated as a function of the individual water flow rates. Fitting each water flow rate as a different data set could increase the R^2 value; however, doing so would not generate results which would rationalize the added complexity.
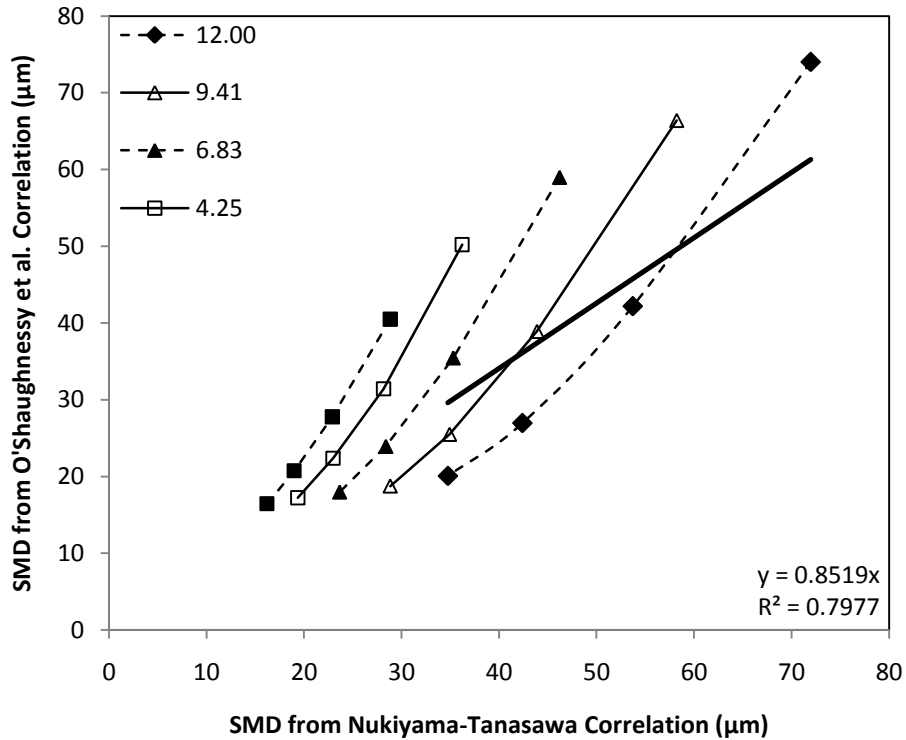
Figure 32. SMD comparison for h = 0.137 in. using C_1 = 1.1000 and C_2 = 0.0093 with trends for water volumetric flow rates in CCM.

Using the results from the O'Shaughnessy *et al.* correlation, Equation 9, and the C_1 and C_2 values shown above, better approximations of the predicted SMD values (shown in Figure 33) for the prototype injector testing can be made. As can be seen in the figure, the general trend of decreasing SMD with increasing AFR is observed for all of the injector distances. However, the wide range of AFR values demonstrated in Figure 33 is not representative of the testing which will be performed in the CRL and makes it difficult to discern trends in the data. To remedy this, Figure 34 shows the predicted SMD values over a smaller range of AFRs.
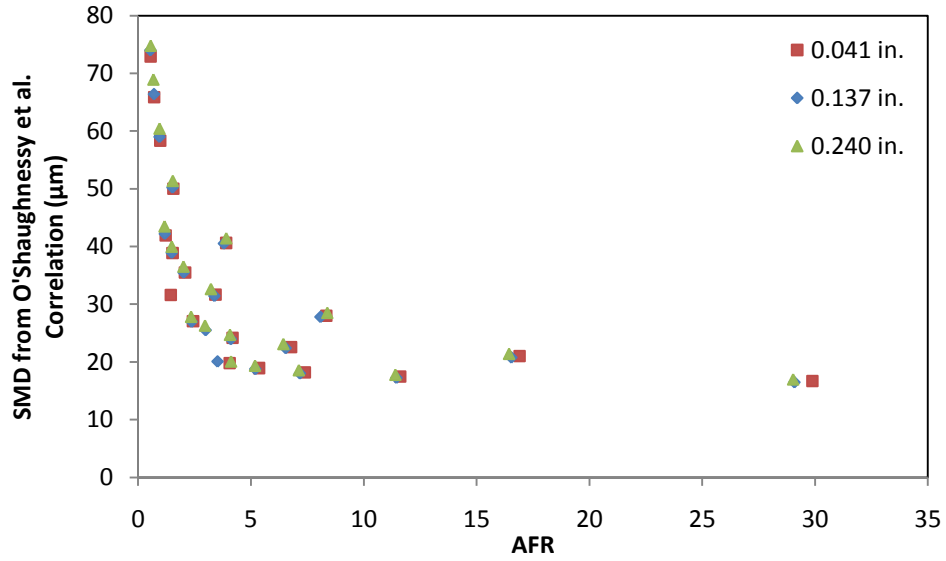
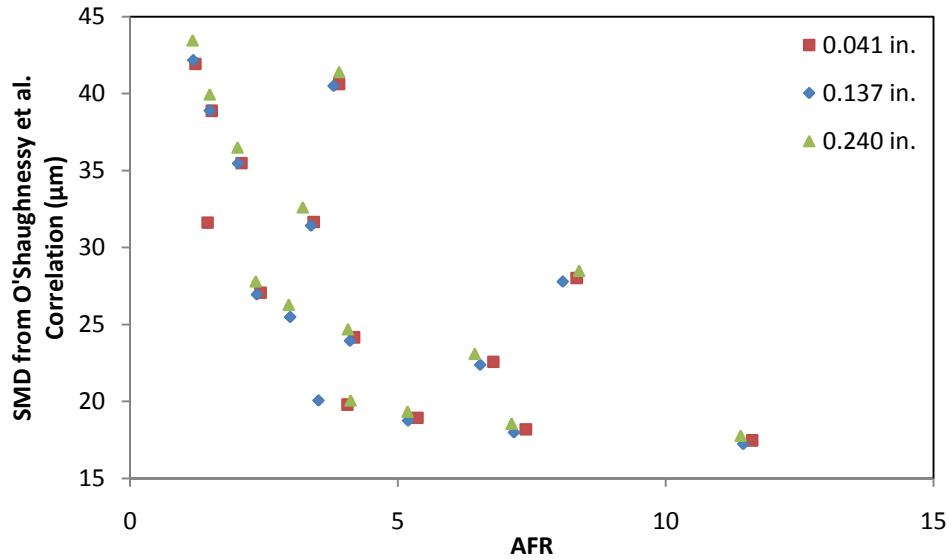**Figure 33.** SMD from the O'Shaughnessy *et al.* correlation as a function of AFR.

Figure 34. SMD from the O'Shaughnessy *et al.* correlation as a function of AFR for a smaller range of AFRs applicable to combustion research.

Figure 34 shows the effect of injector distance, h, on expected SMD. This plot demonstrates that the data appear to cluster around certain points, a trend supported by

the photographic data. A series of images at an approximate AFR of 3.40 and SMD of 32 μm is shown in Figure 35.

Water: 9.41 CCM, Air: 15.78 LPM, Injector Distance: 0.041 in.

Water: 4.248 CCM, Air: 11.31 LPM, Injector Distance: 0.137 in.

Water: 4.248 CCM, Air: 11.31 LPM, Injector Distance: 0.240 in.

Figure 35. Series of images at an AFR of 3.40 and SMD of 32 μm.

The images shown in Figure 35 appear to demonstrate a fully developed flow at each test condition, supporting the similar SMD values estimated by the O'Shaughnessy *et al.* correlation. This suggests that the impact of injector distance – at least when not at extremes – does not have a significant impact on atomization when tests are performed at equivalent AFRs.

Similar to the discussion of the relationship between the two SMD correlations, Figure 33 and Figure 34 display the data as scatterplots without indication of a relation between the clusters of points. The data demonstrate that injector distance does not play a significant role in the expected SMD, so any one data set can be used to more clearly express the impact of increased AFR and water flow rate. This is shown in Figure 36, an adaptation of Figure 34 with trendlines for water flow rates and data for only one injector distance, 0.041 inches.
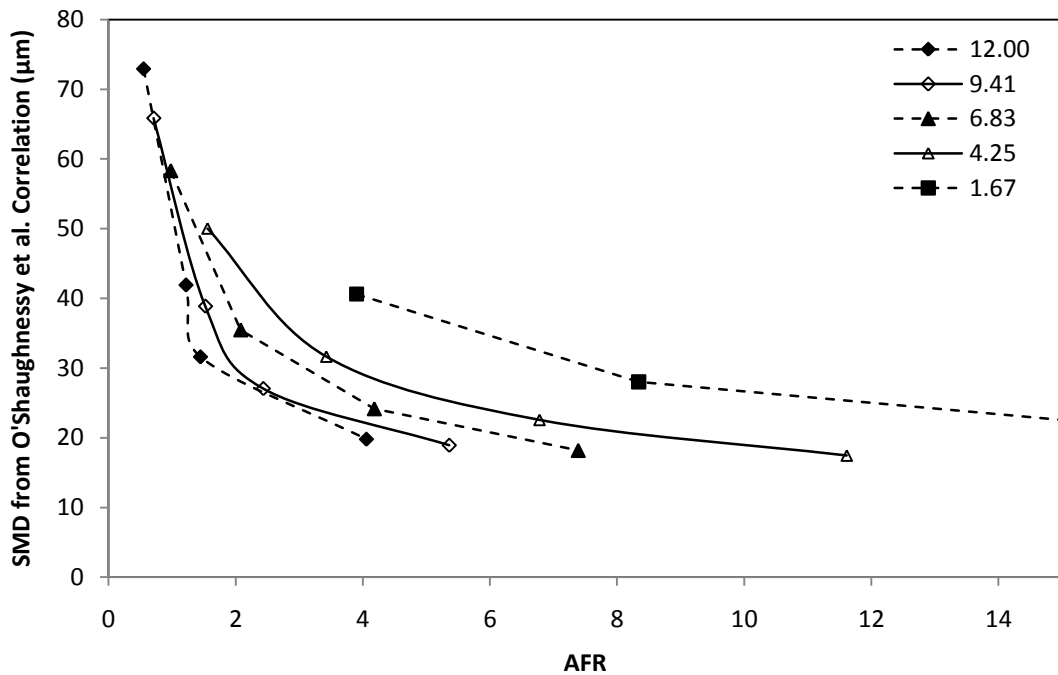

Figure 36. SMD from the O'Shaughnessy *et al.* correlation as a function of AFR for a range of water flow rates in CCM at h = 0.041 inches.

Figure 36 demonstrates that, as the water flow rate decreases, the initial SMD decreases. Also, a small increase in AFR generates a smaller decrease in SMD as the AFR reaches a higher value. By utilizing information derived from this figure, exact AFR values can be estimated for a specific fuel flow rate in the CRL to develop desired SMDs. This is crucial to performing liquid-fuel research.

DESIGN OF NEW INJECTOR

Choosing h = 0.040 inches

The prototype testing and data analysis demonstrated the ability of the injector concept to atomize liquid effectively, but a final determination of the injector distance, h, was necessary for the new design. While attempting to study the impact of an injector distance smaller than 0.041 inches, the effect of having too small of a value was found when set to h = 0.029 inches. As shown by Figure 37, the spray is atomizing the instant it is emitted from the injector. This alone is not necessarily a dangerous result, but the image shows that the flow does not appear to be atomizing properly, with many large droplets spreading out of the tip of the injector. Also, this injector distance created such a small space for the air and water to exit that the atomization air was unable to reach its desired flow rate due to the increased pressure. At 3.1 percent of the available air flow, the maximum available air pressure was reached. Lowering the injector distance below 0.040 inches appears to run the risk of improper atomization.

Figure 37. Image of injector at h = 0.029 inches, 14.56 CCM water, and 5.72 LPM air.

To determine if minute changes in injector distance impact atomization, a test was run at h = 0.039 inches. As shown by Figure 38, this small change did not alter the spray pattern significantly from that for the injector distance of 0.039 inches shown in Figure 24 at similar flow conditions.

Figure 38. Spray-pattern image at an injector distance of 0.039 inches at 9.41 CCM water and 15.78 LPM air.

With these factors in mind, the final injector design parameters were selected. The injector will use h = 0.040 inches, an outer orifice diameter of 0.040 inches, and a liquid-fuel orifice diameter of 0.005 inches. A CAD model of the final design was produced using ProENGINEER. An exploded, cross-sectional view of the injector is shown in Figure 39, and a cross-sectional view of the injector mounted on the 0.25-inch fuel and 0.375-inch air lines is shown in Figure 40.
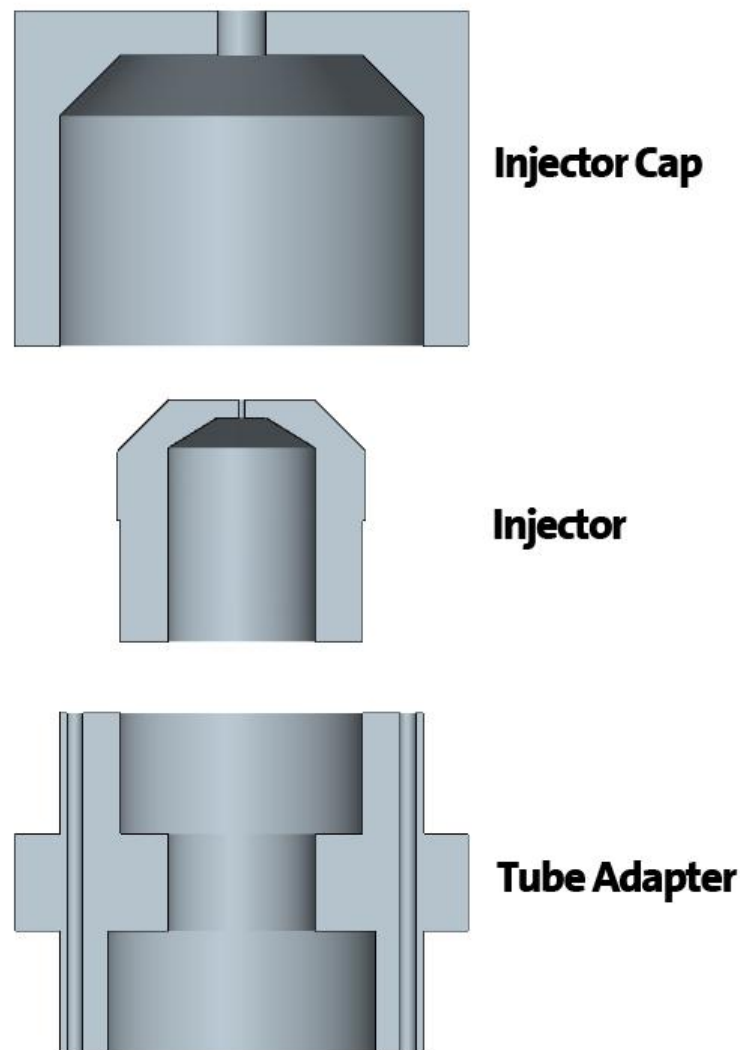

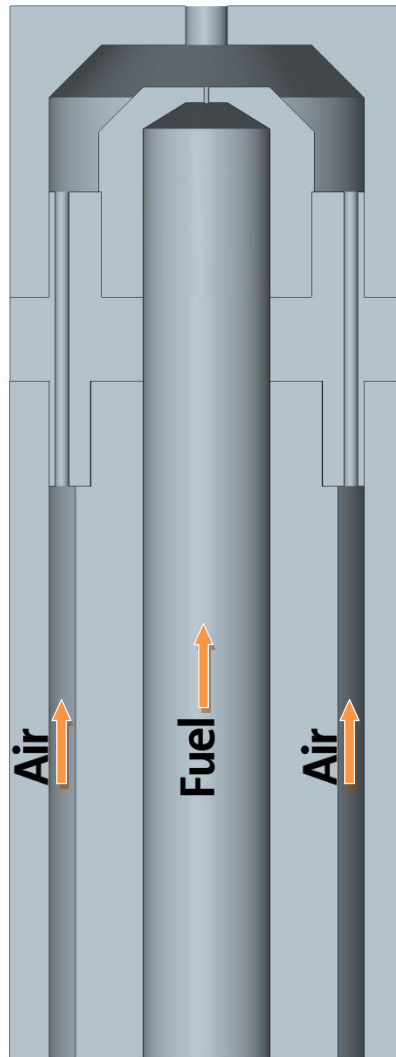**Figure 39.** Exploded view of new injector.

Figure 40. Cross-sectional view of new injector mounted on tubing.

The injector was designed to best fit the CRL's atmospheric combustor system. The components were designed to minimize pressure drop and provide maximum operability. The injector cap is bored out up to the tip to minimize pressure losses from viscous effects along the length of the part. If the 0.005-inch hole ran the full length of the part – instead of the cored section – there would be a significant pressure loss.

Also, the air holes on the sides of the tube adapter are made as short as possible for the same reason. In both cases, the component should be easier to machine because many of these holes will be manufactured using electric discharge machining (EDM), requiring smaller depths. The air holes (as shown in Figure 41) were designed to have an equivalent area much larger than that of the orifice cap to mitigate the pressure drop across the tube adapter.
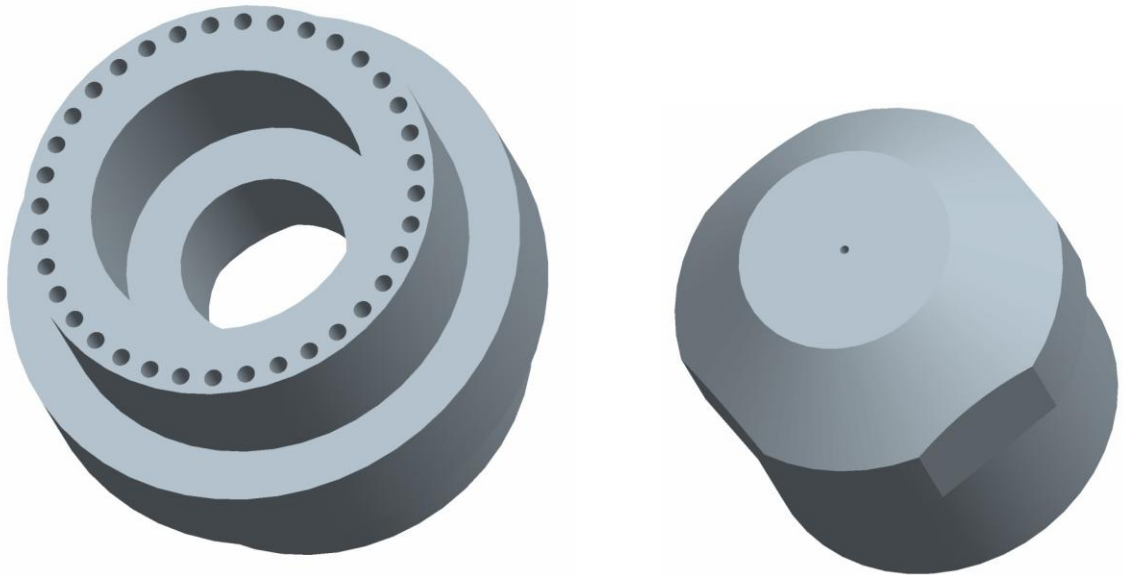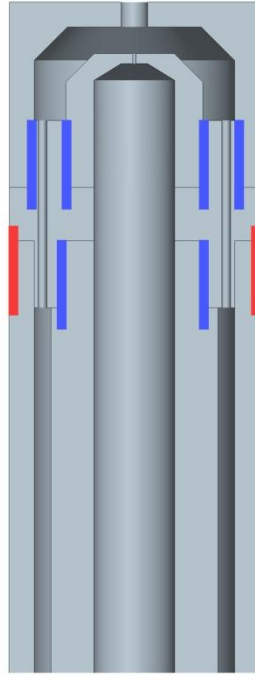

Figure 41. Injector tube adapter (left) and injector (right).

ProENGINEER, the CAD package used to design these components, does not display threads, so Figure 42 indicates where components will be threaded or welded together during assembly. To facilitate removal of the injector cap, the four sides were squared off, as shown in Figure 41.

Figure 42. Cross-sectional view of new injector mounted on tubing with machining placement.

CONCLUSIONS AND FUTURE WORK

A concept for a new liquid-fuel injector for the Combustion Research Laboratory at Bucknell University was conceived, evaluated experimentally through testing of a prototype, and a CAD model of the final proposed design was created. The main goal of the new injector design is to alleviate the high pressure and high volumetric flow rate that is required to achieve proper atomization of liquid fuel with the current nozzle. Eventually, the new injector will be manufactured by the machine shop during summer 2011 and will be tested shortly thereafter. Once the new injector is deemed satisfactory, it will be used in the CRL's liquid-fuel system in alternative fuel combustion tests.

A study of the new system's attributes, particularly its resistance to coking and the pressure drop across the injector, will be performed at various flow rates with heptane. The flame characteristics can be observed visually, recorded with digital photography, or studied with a photomultiplier tube, a highly sensitive light detector. After the baseline data is collected from heptane, other fuels such as JP-8 (a standard military jet fuel) and Fischer-Tropsch fuels will be tested to investigate the fuel flexibility of the new injector. Later, utility of the new injector at PERC will be evaluated by scaling up its size relative to the larger flow requirements of the PERC system.

REFERENCES

[1] Hamelinck, C., Faaij, A., den Uil, H., and Boerrigter, H., 2004, "Production of FT transportation fuels from biomass; technical options, process analysis and optimisation, and development potential," Energy, 29 (11), pp. 1743-1771.

[2] Corporan, E., DeWitt, M.J., Belovich, V., Pawlik, R., Lynch, A. C., Gord, J.R., and Meyer, T.R., 2007, "Emissions Characteristics of a Turbine Engine and Research Combustor Burning a Fischer-Tropsch Jet Fuel," Energy and Fuels, 21 (5), pp. 2615-2626.

[3] Weaver, D., 2010, "Design, Construction, and Validation of an Atmospheric Combustor for Alternative Fuel Studies," Honors Thesis, Bucknell University, Lewisburg, PA.

[4] Pierce, W., 2010, "Combustion of Biogas in a Gas Turbine Simulation," Graduate Thesis Proposal, Bucknell University, Lewisburg, PA.

[5] Turns, S., 2000, *An Introduction to Combustion: Concepts and Applications,* 2nd Edition, McGraw-Hill Higher Education, New York, NY.

[6] Jasuja, A.K., 1979, "Atomization of Crude and Residual Fuel Oils," Transactions of the ASME, 101, pp. 250-258.

[7] Lefebvre, A., 1989, *Atomization and Sprays*, Hemisphere Publishing Corporation, New York, NY.

[8] Lefebvre, A., 1980, "Airblast Atomization," Progress in Energy and Combustion Science, 6, pp. 233-261.

[9] Jasuja, A.K., 1982, "Plain-Jet Airblast Atomization of Alternative Liquid Petroleum Fuels Under High Ambient Pressure Conditions," International Gas Turbine Conference and Exhibit, 27.

[10] Bartok, W. and Sarofim, A., 1991, *Fossil Fuel Combustion: A Source Book*, John Wiley & Sons, Inc., New York, NY, Chap. 9.

[11] Cengel, Y.A., and Cimbala, J.M., 2010, *Fluid Mechanics: Fundamentals and Applications*, 2nd Edition, McGraw-Hill, New York, NY.

[12] O'Shaughnessy, P., Bideau, R., and Zheng, Q., 1998, "Injector Geometry Effect on Plain Jet Airblast Atomization," Proceedings of the 1998 International Gas Turbine & Aeroengine Congress & Exhibition, 445.

[13] Omega. Flow Data for Omega FL-3439ST. *Document No. 528.*